ARL-TR-8019 ● MAY 2017

US Army Research Laboratory

Sensing Applied Load and Damage Effects in Composites with Nondestructive Techniques

by Colleen Rosania, Mulugeta A Haile, Natasha C Bradly, Asha Hall, Michael Coatney, and Fu-Kuo Chang

NOTICES

Disclaimers

The findings in this report are not to be construed as an official Department of the Army position unless so designated by other authorized documents.

Citation of manufacturer's or trade names does not constitute an official endorsement or approval of the use thereof.

Destroy this report when it is no longer needed. Do not return it to the originator.

ARL-TR-8019 ● MAY 2017

US Army Research Laboratory

Sensing Applied Load and Damage Effects in Composites with Nondestructive Techniques

by Mulugeta A Haile, Natasha C Bradly, Asha Hall, and Michael Coatney
Vehicle Technology Directorate, ARL

Colleen Rosania and Fu-Kuo Chang
Department of Aeronautics and Astronautics, Stanford University, Stanford, CA

REPORT DOCUMENTATION PAGE

Form Approved
OMB No. 0704-0188

1. REPORT DATE *(DD-MM-YYYY)*	2. REPORT TYPE	3. DATES COVERED (From - To)
May 2017	Technical Report	January 2016–February 2017

4. TITLE AND SUBTITLE
Sensing Applied Load and Damage Effects in Composites with Nondestructive Techniques

5a. CONTRACT NUMBER

5b. GRANT NUMBER

5c. PROGRAM ELEMENT NUMBER

6. AUTHOR(S)
Colleen Rosania, Mulugeta A Haile, Natasha C Bradly, Asha Hall, Michael Coatney, and Fu-Kuo Chang

5d. PROJECT NUMBER

5e. TASK NUMBER

5f. WORK UNIT NUMBER

7. PERFORMING ORGANIZATION NAME(S) AND ADDRESS(ES)
US Army Research Laboratory
ATTN: RDRL-RDRL-VTM
Aberdeen Proving Ground, MD 21005-5066

8. PERFORMING ORGANIZATION REPORT NUMBER
ARL-TR-8019

9. SPONSORING/MONITORING AGENCY NAME(S) AND ADDRESS(ES)

10. SPONSOR/MONITOR'S ACRONYM(S)

11. SPONSOR/MONITOR'S REPORT NUMBER(S)

12. DISTRIBUTION/AVAILABILITY STATEMENT
Approved for public release; distribution is unlimited.

13. SUPPLEMENTARY NOTES

14. ABSTRACT

Composite materials are desirable for many aerospace applications but pose challenges due to their complicated damage mechanics. Implementing a structural health monitoring (SHM) strategy for composite structures is one approach for assessing the health or damage state in real time. Application of SHM requires not only the ability to localize, classify, and quantify damage, but also compensate for changing environmental and operating conditions. One such problem is compensating for the effects of applied load on a composite structure to correctly estimate damage. To study the effects of applied load, composite coupons were tested in static and fatigue loading, gathering data in various damage and loading states with multiple nondestructive evaluation (NDE) techniques. Evaluation using piezoelectrically induced guided waves, acoustic emission, thermography, and X-ray imaging were compared and correlated. This report summarizes experimental setups involving the various NDE methods and technics and provide results on the effects of load and damage in the received ultrasonic signals.

15. SUBJECT TERMS
guided waves, feature extraction, NDE, fatigue, acoustic emissions

16. SECURITY CLASSIFICATION OF:			17. LIMITATION OF ABSTRACT	18. NUMBER OF PAGES	19a. NAME OF RESPONSIBLE PERSON
a. REPORT	b. ABSTRACT	c. THIS PAGE			Mulugeta A Haile
Unclassified	Unclassified	Unclassified	UU	40	19b. TELEPHONE NUMBER (Include area code) 410-278-5289

Standard Form 298 (Rev. 8/98)
Prescribed by ANSI Std. Z39.18

Contents

List of Figures

List of Tables

1. Introduction

1.1 Motivation

Composite materials are desirable for aeronautical and aerospace applications for many reasons including their high strength-to-weight ratios, fatigue and corrosion resistance, design adaptability, and performance capabilities in harsh environments.[1–5] Because of these qualities composites are useful in many applications such as in armor, helmets, and helicopters, and as structural components. However, when in-service composite materials experience very different damage mechanics than metals. Performance and quality of composite materials can suffer from fatigue, environmental conditions, and external damage just as metals, but due to their inherent complexity and the difficulty of detecting damage in composites with traditional inspection techniques, maintaining and guaranteeing the safety of composite structures is a challenging problem. Strategies such as structural health monitoring (SHM), a system with which to monitor a structure in real time, are particularly useful for composite materials, because they combat these difficulties by giving warning of any changes to the system. Implementing reliable SHM strategies into composite structures will allow the Army to fully take advantage of the performance capability of composite materials while increasing efficiency by saving time and expense on repair, decreasing the need to take structures out-of-service for inspection, decreasing the occurrence of sudden failures, and extending the lifetime of composite structures by enabling efficient maintenance. This project studies damage progression in composite materials as monitored by multiple techniques used in nondestructive inspection to further understanding of the material itself and the capabilities of various nondestructive evaluation (NDE) techniques. Correlating and validating NDE strategies for sensing damage and operational effects on composite materials will add to the knowledge of composites and efficient strategies to monitor these materials and use them to their full capabilities.

1.2 Composite Materials

There are many types of composites used in industry based on materials such as glass fiber, Kevlar, and carbon fiber combined with various types of epoxy.[4,6] Carbon fiber-reinforced polymers are particularly useful in necessarily low-weight but high-strength applications. Unidirectional prepreg composites, which have fibers oriented in the same direction held together by an epoxy matrix, are one of the most commonly used of these materials. Individual plies can be oriented and

stacked together to create a laminated composite structure with specific material properties.[7,8] Figure 1 illustrates an example of a laminated composite of unidirectional plies. In this way, a designer can create a composite laminate with tailored material properties necessary for a specific application.

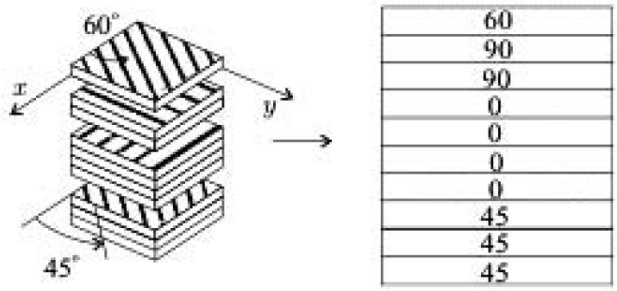

Fig. 1 Example of a layup of a laminated [$45_3/0_4/90_2$/60] composite of unidirectional plies, with schematic (left) and stacking order (right)[8]

This unique design capability and adaptability coupled with potential high strength-to-weight ratios make composite materials extremely desirable for high-performance applications. However, composites have relatively complicated and situation-dependent damage mechanics. Composite materials experience multiple damage types that can occur together or in sequence to contribute to a weakened structural state or final failure. The main modes of failure are matrix cracking, delamination, fiber breakage, and fiber buckling, which all can contribute individually or together to the progressive degradation and weakening and then final failure of a composite structure. In fatigue loading, the types of failure that predominantly occur and are a signal of potential areas for final failure are matrix cracking and delamination.[8–12]

1.3 Damage in Composites

Matrix cracking is often the first type of failure to occur in a composite laminate and is a precursor to other types of failure. It does not result in the final failure of the composite but does contribute to strength degradation in the laminate. Matrix cracking is a matrix-dominated failure, which occurs in the matrix between individual fibers and perpendicular to the fiber direction, as shown in Fig. 2. Once a matrix crack appears, it quickly spreads through the entire width of the material. Matrix cracks can form due to fatigue, impact, or thermal stress mismatch between plies, which can occur during manufacturing. Matrix cracking decreases a ply's stiffness and strength, which contributes to the degradation of the global stiffness and strength of the composite. The increasing density of matrix cracks in a ply lead

to increased stress mismatch between plies, which in turn causes delamination. In this way a high density of matrix cracks can "spread" to between the plies due to the interfacial stress mismatch, forming a region of delamination.[8,9,13,14]

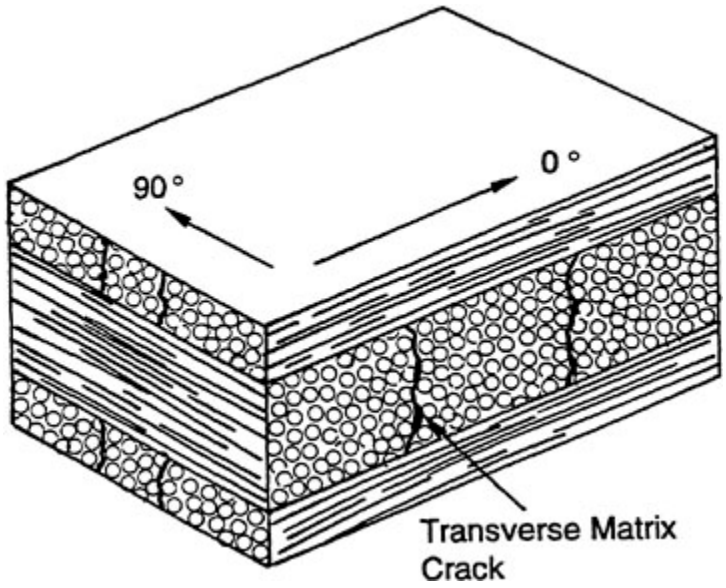

Fig. 2 Representation of the formation of transverse matrix cracks in a cross-ply laminate[15]

Delamination is a type of composite damage that can result in final failure of a composite laminate. Delamination refers to separation between adjacent plies in a layup (Fig. 3), which can form during manufacture or as a result of loads during use. Results of delamination include a reduction in stiffness, strength, and load-carrying capability of the composite. Repeated loading on a composite laminate with internal delamination causes growth of the area damage, which may result in complete failure of the composite structure. There exists a critical stage of delamination for each application after which the growth of the delamination becomes unstable, much like the growth of cracks in metals, which can result in rapid failure. This makes delamination a critical damage type to sense and monitor in composite structures in use.[8]

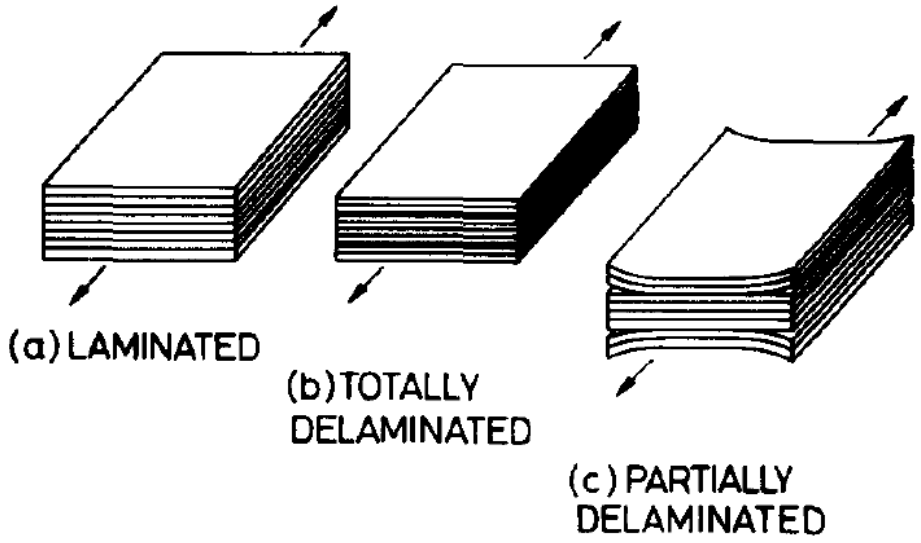

Fig. 3 Schematic of different states of delamination in a composite laminate[16]

Traditional failure mechanics and inspection techniques used with metals do not work when applied directly to composite materials because of their inherent differences. NDE techniques exist that can evaluate composite structures for damage including C-Scan, radiography, thermography, shearography, and laser ultrasonics. However, these technologies are cumbersome and time-consuming, often requiring a structure to be disassembled to inspect all components. Additionally, composites' layered construction, tendency for subsurface damage, and complicated damage mechanics make damage assessment challenging especially due to the fact that there is no established NDE regimen across the board to evaluate composite materials.[17–20] Finally, composite materials can suffer a lot of internal damage and subsequent stages of weakening in the structure before final failure occurs.[8,21] Therefore, damage progression is harder to predict in addition to being more difficult to detect with current NDE technologies.

1.4 Structural Health Monitoring

One solution to this problem is using SHM strategies for composites (i.e., integrating a strategy into the composite structure with which to detect damage and state in real time). The idea is to observe the system or structure over time to gather data about the system and from measurements extract features that are sensitive to damage. By using statistical methods to track changes in damage-sensitive features throughout the life of the structure, the current state of health can be determined. Depending on the application, SHM can be used to observe long-term slow progression of damage such as fatigue or extreme events such as impacts.[22] There are many methods for implementing SHM systems,[23-27] and multiple NDE

techniques are used in this study for mutual correlation and verification. The following subsections discuss the methods compared.

1.4.1 Guided Wave-Based SHM

Guided ultrasonic waves can be propagated through a structure to gather information about changing conditions in the material. Ultrasonic waves can be excited through a composite structure by attaching or embedding ultrasonic transducers, such as piezoelectric elements, to the material. Applying voltage to a piezoelectric transducer causes corresponding strain in the piezoelectric material, and when the transducer is attached on or embedded in a material, this instigates a wave of elastic deformations that propagate through the material and can be detected by another piezoelectric element. When a disturbance such as a guided ultrasonic wave interacts with the piezoelectric element causing strain deformation, the opposite effect occurs, producing an output voltage that can be collected and analyzed. When these properties are used, a small number of these sensors can scan relatively large areas by introducing the wave at one point and sensing in another, therefore detecting changes along a certain propagation path.[28]

Properties of ultrasonic waves depend on the medium through which they propagate. The material properties of the host structure, such as the stiffness and density, affect the wave velocity and also the dispersion of the wave as it travels through the material. Because of wave dispersion and attenuation the amplitude and energy content of the wave changes as it propagates. Specifically in this case, analysis is focused on Lamb waves, a type of guided ultrasonic wave that propagates in plate-like panels in 2 categories of modes, symmetric and antisymmetric. As Lamb waves are through-thickness waves, collected data include information on material properties, damage, and material state through the entire thickness of the material along a travelled propagation path.[29–31]

Damage in a structure affects wave propagation because when waves interact with a structural discontinuity such as damage, it causes reflections, scatter, and energy loss. The global plate properties of stiffness and damping are also affected by damage, which in turn affects wave propagation. Additionally, environmental and operational changes will affect these same global properties and therefore wave propagation. The gathered voltage data from piezoelectric sensors include these differences in wave propagation as the structure changes, which can be analyzed for SHM.[22,28]

1.4.2 Acoustic Emission

Acoustic emission (AE) relies on the same basic principles of guided waves, namely, that vibrations travelling through a material can be detected and analyzed. However, where guided wave-based SHM is an active form of SHM, in that a signal is applied to the system to induce a response, AE is passive in that it senses vibrations naturally generated by the material. When events such as matrix cracking, fiber-matrix debonding, delamination, or fiber breakage occur in a composite material, stress waves result from these defects. An array of highly sensitive piezoelectric elements can detect these events as they propagate concentrically from their origin point. AE is a valuable method because of both its passive nature, not requiring any input signals to operate, and its ability to detect dynamic processes occurring in the material, therefore differentiating between static and developing defects. Though advantages of AE include its high sensitivity to multiple types of events and ability for global inspection, advanced methods are required to interpret and correlate AE data to specific damage mechanisms.[17,19,20]

1.4.3 Thermography

Thermography, also known as thermal imaging, uses the fact that the thermal conductivity of a material may change when defects are present. A rapid heat pulse is applied to a specimen's surface, causing a temperature rise on the surface. Given a short enough pulse, temperature diffusion is governed solely by the material. Any inhomogeneity in the material in the form of manufacturing defects or damage will appear as temperature differences. Flaws such as delamination cause a change in the thermal radiation in their local area causing these changes. Advantages of thermography include being noncontact and its ability to inspect large areas, while disadvantages include the necessity of expensive and sensitive equipment, highly skilled operators, and the fact that defects deep below the surface will be obscured.[17,19,20]

1.4.4 X-Radiography

Using X-rays for inspection is the most common testing method. In combination with X-ray opaque dye penetrants, which illuminate damage in the images, X-ray imaging is an accurate way of detecting damage in a composite material not visible to the naked eye. As one of the oldest and most established forms of inspection widely understood across multiple disciplines, X-radiography is often used in conjunction with other NDE methods as a way to validate SHM techniques. Though X-rays are useful and reliable for validation, on a large scale or onboard a system, they are impractical due to the harmful nature of the radiation.[19,20,27]

2. Experimentation

A series of experiments were conducted to collect NDE data at different applied load levels and progressive damage states eventually through the fatigue life of composite coupons. Multiple composite samples of the chosen layup were instrumented with piezoelectric elements and loaded in tension-tension fatigue to induce first matrix cracking and then delamination in the material. NDE data were collected in both loaded and unloaded conditions at each damage state, and X-ray images were taken at each interval to assess current damage. The experiments are described in detail in the following sections.

2.1 Composite Test Samples

All composite coupons were composed of Torayca T700G/2510 unidirectional carbon fiber prepreg material. Unidirectional ply properties were given by the manufacturer and are shown in Table 1. The composite coupons for this experimental series were manufactured by Composites Universal Group. They were vacuum bagged and oven cured and then water-jet cut to experimental specifications. Glass fiber tabs approximately 2 inches in width were attached to the top and bottom of the coupons for clamping during testing. The manufacturer's specifications sheet reported a void content of 5%–7% in the laminates, and though this will lead to variability between the coupons and in the experimental results, the material and manufacturing process are approved by the Federal Aviation Administration for use in aircraft.

Table 1 Material properties of a T700G/2510 unidirectional composite ply

Property	Value
E_1 (Msi)	18.5
E_2 (Msi)	1.2
G_{12} (Msi)	0.9
G_{23} (Msi)	0.5
ν_{12}	0.3
ν_{23}	0.22
h (ply thickness, inches)	0.00625

A cross-ply laminate was used in this experimental series. This layup was chosen due to its high-fatigue resistance such that a density of matrix cracks form in the 90° plies in the laminate prior to delamination, and that damage will be easily visible on X-ray images. The chosen layup was a $[0_2/90_4]_S$ cross-ply laminate (0.075 inches thick). The geometry used is of a "necking" or "dogbone" configuration. Each coupon has a notch cut into the left edge at the center of the

coupon. Notched samples develop matrix cracking and delamination quickly due to the notch serving as a damage initiation point. The dimensions of the coupons are shown in Fig. 4.

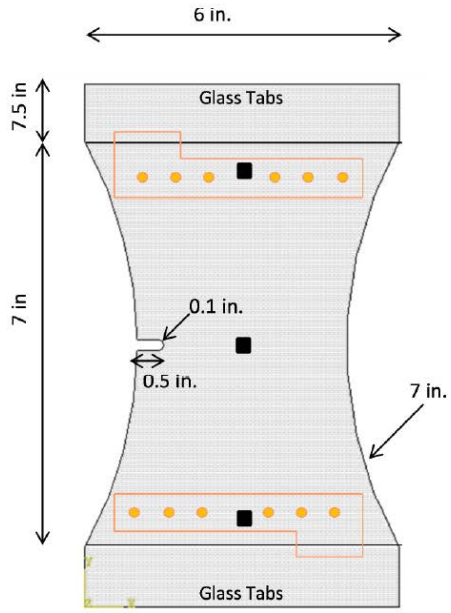

Fig. 4 Dimensions of the composite coupon geometry[28]

2.2 Piezoelectric Sensor Networks

Piezoelectric elements were attached on the surface of each composite coupon to the top and bottom of the coupon to act as actuators and sensors respectively (as shown in Fig. 4). Twelve piezoelectric elements were attached to each coupon in the form of two 6-lead zirconate titanate (PZT)-sensor SMART Layers from Acellent Technologies, Inc.[34] The SMART Layers consist of 1/4-inch-diameter, 0.007-inch-thick piezoelectric discs, which are layered in a dielectric film with wiring for data collection. The SMART Layers were adhered to the surface of the composite coupons using aerospace-grade adhesive. The SMART Layers were placed approximately 3 inches from the center of the notched coupons. Actuator and sensor coordinates were recorded for each sample with reference to the bottom-left corner of the coupon, as shown with the coordinate axes in Fig. 4.

Ultrasonic data were actuated and collected using an Acellent ScanSentry 32-channel data acquisition system paired with a computer with ACESS interface software. Figure 5 shows a photograph and diagram example of the experimental setup with a notched coupon. Piezoelectric elements were numbered for each coupon as shown in Fig. 5 with elements 1–6 at the top of the coupon acting as

actuators and elements 7–12 at the bottom of the coupon acting as sensors. With this configuration, 36 total propagation paths with varying path angles were used for data collection.

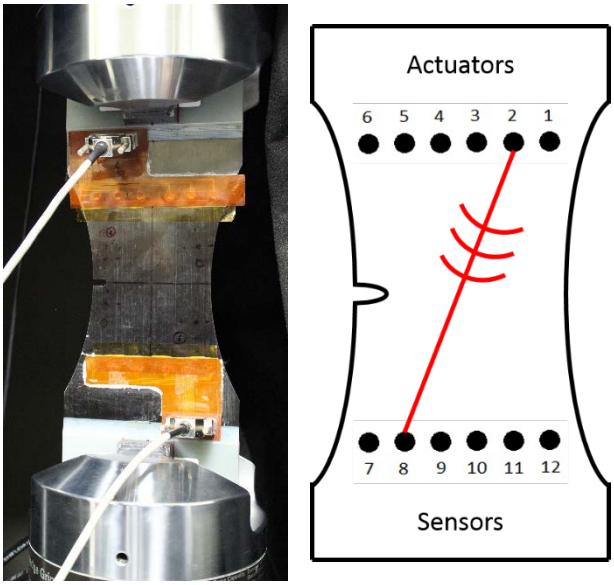

Fig. 5 Experimental setup with a composite coupon loaded in a mechanical testing system (MTS) machine (left) and the sensor schematic with example wave propagation (right)

2.3 Data Collection

At each data collection point Lamb waves were propagated from each actuator to each sensor, adding up to a total of 36 paths of information to analyze for each actuation frequency at each time point. The actuation signal was a 5-peak Hanning-windowed tone burst signal with a center frequency ranging from 150 to 450 kHz. The average input voltage for each signal was 50 V and the average gain was 20 dB, though actuation parameters were varied for each actuator-sensor event such that the amplitude of the sensed signal was approximately 0.8 V to avoid saturating the sensing system. To choose and verify the wave modes present from these propagation signals, dispersion curves for these composite plates were computed using Disperse software (by Dr Cecilia Wilson). When these actuation frequencies were used, data with distinguishable fundamental symmetric and antisymmetric modes were collected. The testing apparatus is shown in Fig. 6.

Fig. 6 Photographs showing a composite sample loaded for testing with AE sensors (left) and the thermographic imager and cables attached for ScanSentry data collection (right)

After each stage in testing the sample was removed from the testing apparatus to take an X-ray image to quantify the current damage. As discussed previously, damage in composite coupons is often internal and therefore NDE methods are required to "see" this "invisible" damage. X-ray images of the composite coupons were taken at Chesapeake Testing with an industrial X-ray and computed tomography (CT) machine. Coupons were treated with an X-ray opaque dye penetrant, 1,4 diiodobutane, which enhances X-ray absorption to illuminate damage on the images.[27,30]

2.4 Testing Procedure

Testing on all coupons begins with static loading, which progresses into tension-tension fatigue testing. Initial loading is done slowly and in steps to capture data while the composite sample is under loading but before damage appears. These initial data can be used to study the isolated effects of applied load on the various types of NDE. Additionally, slow initial loading allows slow progression of damage in the sample, allowing the collection of data containing only effects of matrix cracking and later data influenced by delmaination. Table 2 shows the testing process for each coupon. Fatigue settings for the sample are based on static-to-failure tests done previously at Stanford University to determine the ultimate tensile strength of the composite coupons. Maximum fatigue load was set at 70%–80% of the static failure strength of the laminate, and the load ratio (R) for the tests was approximately 0.14. The loading profile for the fatigue tests is sinusoidal at a frequency of 5 Hz. The steps taken during each test are outlined in the following sections.

Table 2 Initial static and fatigue cycle count order for testing of coupons

Test no.	Total cycle count	Cycles for current test	Loading type
1	0	~1/2	Static up to 4 kips, stopping every 0.5 kips for NDE data
2	1	1 (effectively)	Static up to 7 kips, stopping every 0.5 kips for NDE data
3	10	9	Fatigue at 5 Hz: max 7 kips, min 1 kip, mean 4 kips (span 3 kips)
4	100	90	
5	1,000	900	
6	10,000	9,000	
7	20,000	10,000	
8	30,000	10,000	
9	40,000	10,000	
10	50,000	10,000	
11	60,000	10,000	
12	70,000	10,000	
13	80,000	10,000	
14	90,000	10,000	
15	100,000	10,000	
16	125,000	25,000	
17	150,000	25,000	
18	175,000	25,000	
19	200,000	25,000	
20	250,000	50,000	If necessary continue past 250,000 cycles at 50,000 intervals

2.4.1 Static Procedure

1) Take traction-free ScanSentry data.
2) Clamp sample into MTS, make sure to match central aligning marks.
3) Take clamped ScanSentry data, remove cables.
4) Take thermographic image, wait until finished.
5) Attach AE sensors and adjust for noise.
6) Begin collecting AE data.
7) Load sample 0.5 kips at a rate of 0.5 kips/min. The MTS program should be set up to ramp and hold at each load step.
8) Pause AE collection.
9) Remove AE sensors, wipe off gel.
10) Take loaded ScanSentry data and remove cables from sample.
11) Take thermographic image.

12) Reattach AE sensors.

13) Restart AE data collection.

14) Repeat steps 7–13 for up to the second-to-last load step (i.e., through 3.5 or 6.5 kips).

15) Repeat steps 7–11 for the last load step (i.e., at 4 or 7 kips).

16) Unload the sample from the maximum load (4 or 7 kips) at a rate of 1 kip/min.

17) Take clamped ScanSentry data.

18) Unload the sample from the MTS machine.

19) Take traction-free ScanSentry data.

20) Take X-ray of sample before next test.

2.4.2 Fatigue Procedure

1) Take traction-free ScanSentry data.

2) Clamp sample into MTS.

3) Take clamped ScanSentry data, remove cables.

4) Take thermographic image.

5) Attach AE sensors and adjust for noise.

6) Begin collecting AE data.

7) Load sample to 4 kips at a rate of 1 kip/min.

8) Pause AE collection.

9) Remove AE sensors, wipe off gel.

10) Take loaded ScanSentry data and remove cables from sample.

11) Take thermographic image.

12) Reattach AE sensors.

13) Restart AE data collection.

14) Begin fatigue cycling for the number of “Cycles in Current Test” as indicated in Table 1. Fatigue settings are a mean of 4 kips and span of 3 kips (i.e., min 1 kip and max 7 kips) at 5 Hz.

15) Stop AE data collection, remove AE sensors and wipe off gel.

16) Take loaded ScanSentry data and remove cables.

17) Take thermographic image.

18) Unload sample from 4 kips to 0 at a rate of 1 kip/min.

19) Take clamped ScanSentry data.

20) Unload sample from MTS.

21) Take traction-free ScanSentry data.

22) Take X-ray of sample before next test.

2.5 Experiment Results

Table 3 summarizes the 3 samples tested during this study.

Table 3 Summary of completed tests at the US Army Research Laboratory (ARL)

Sample	Test no. completed	Loading completed	Observed damage
L1S01	2	Static: 7 kips	Small delamination and few matrix cracks
L1S02	1	Static: 4 kips	Few matrix cracks
L1S03	1	Static: 4 kips	Few matrix cracks

Examples of an extracted X-ray image and the AE data collected are shown in Fig. 7 and an example of a 3-D X-ray CT of damage is shown in Fig. 8. After the dye penetrant was applied, damage was visible on the X-ray CT scans. Without dye penetrant there was not enough contrast between damaged and undamaged sections for the damage to be visible on X-ray CT. The damage location shown on the X-rays correlates with the observed AE hits during experimentation as shown in Fig. 7.

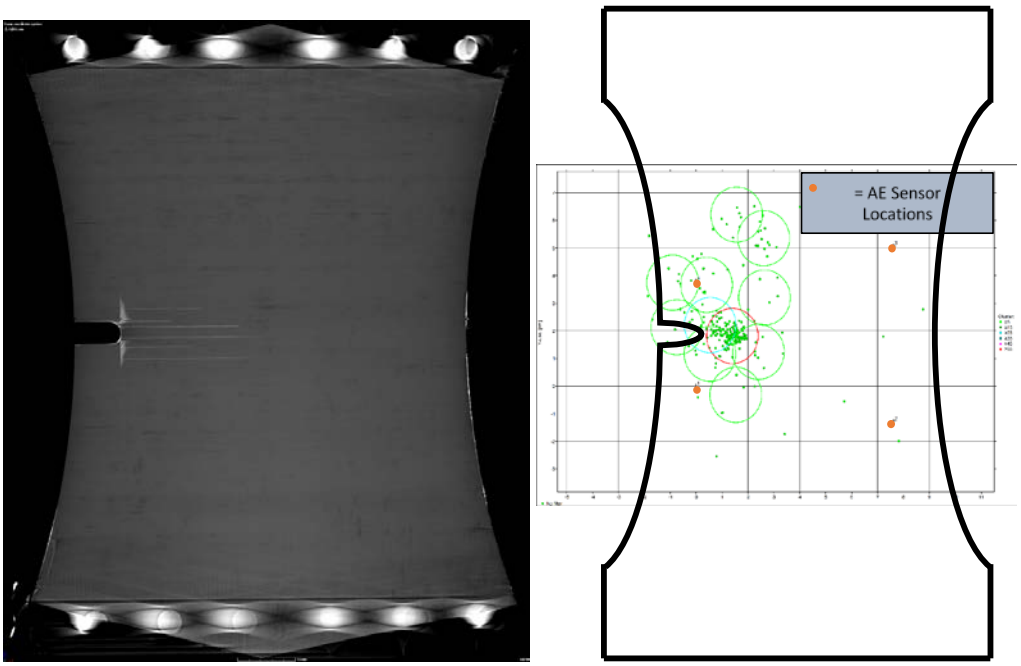

Fig. 7 Extracted X-ray image (left) from the X-ray CT scan of L1S01 after 7 kips loading showing a small delamination and matrix cracking around the notch compared with collected AE hits (right) during the test

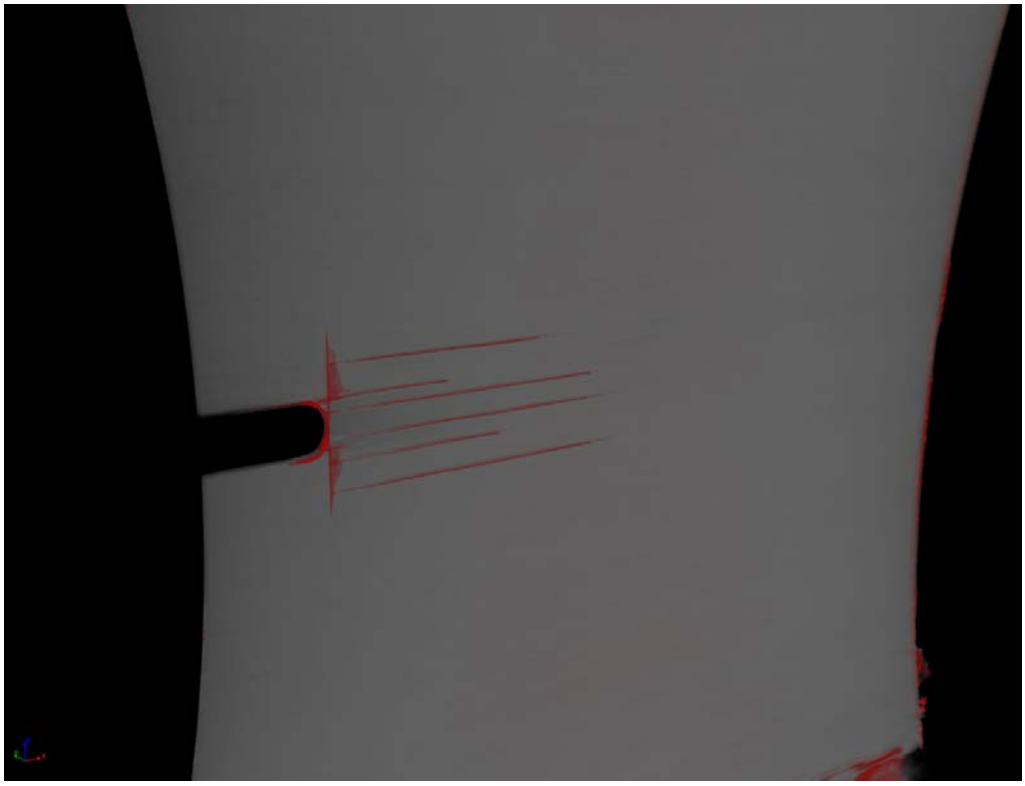

Fig. 8 A 3-D view of the damage in L1S01 after 7 kips loading. The dye penetrant improves contrast between damaged and undamaged sections.

3. Signal Processing

During experimentation, NDE data are gathered in the form of AE data, thermographic images, and guided-wave signals. As stated earlier, one of the main contributions of this report is in the processing and interpreting of the guided-wave data. Future work will included analysis of data from acoustic emission sensors and flash thermography. In this report, we explain the results gathered from the ScanSentry guided-wave data.

3.1 Ultrasonic Signal Response

To assess the effects of load and damage on Lamb waves, the collected wave data must by processed and analyzed. Because guided-wave properties are dependent on the medium through which they propagate—as discussed in Section 1—when the host material is affected by applied load or damage, the wave signal is affected as well. By extracting features from the sensor signal and examining their change over time, parameters sensitive to the applied load and/or present damage can be identified. Qualitatively there are noticeable differences in sensor signal when it is effected by applied load and different levels of damage. Following are examples of raw sensor signal showing some of these variations. Figures 9 and 10 show how increasing levels of applied load on a coupon effect guided-wave data propagating through that coupon without damage effects.

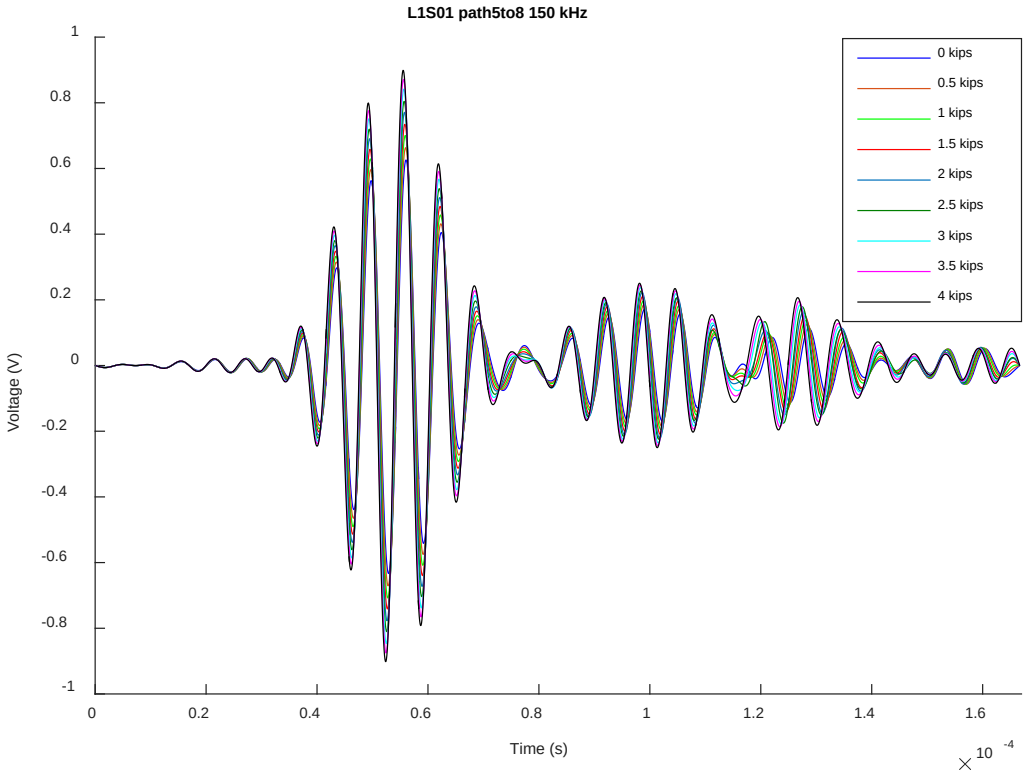

Fig. 9 Raw signal of L1S01 from path 5to8 at 150-kHz actuation frequency as the load increases from 0 to 4 kips

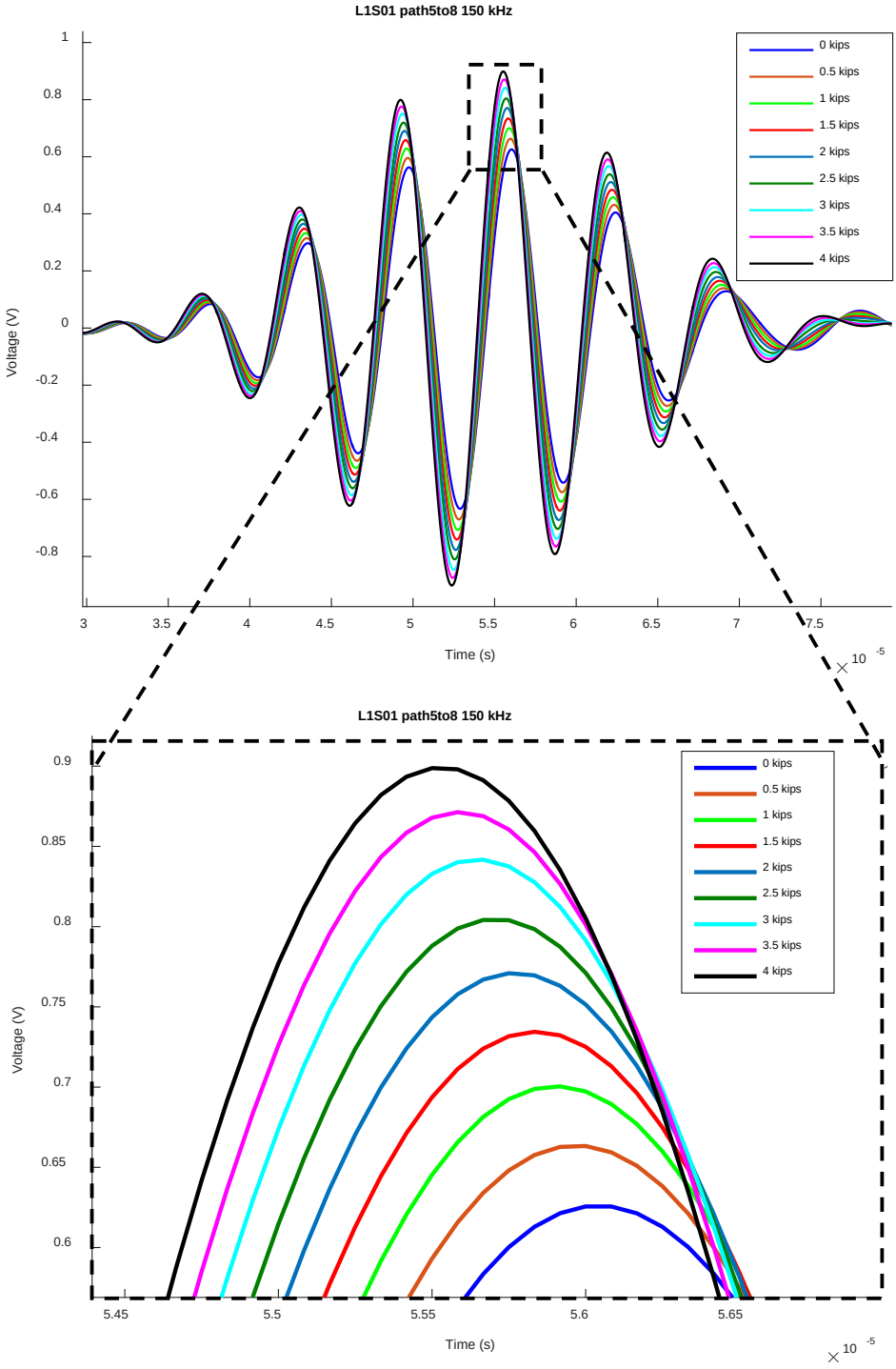

Fig. 10 Zoom in of the first wave packet (top) and one peak (bottom) of data collected from L1S01 path 5to8 as the load increases showing the change in sensor signal (no damage present)

3.2 Feature Extraction

Based on initial raw data analysis and dispersion curves created pre-experiment, the most consistently clear wave packet was the first arrival, the S_0 mode. Figure 11 shows an example of the sensed signal from an actuator-sensor pair with the actuation frequency of 150 kHz. In each data set, the first arriving wave packet is identified, as shown in Fig. 11, and analyzed for signal parameters in the time and frequency domains. Figure 12 shows the amplitude (*A*) and time of fight (TOF) were studied in the time domain and are extracted from the window enclosing the first arriving wave packet.

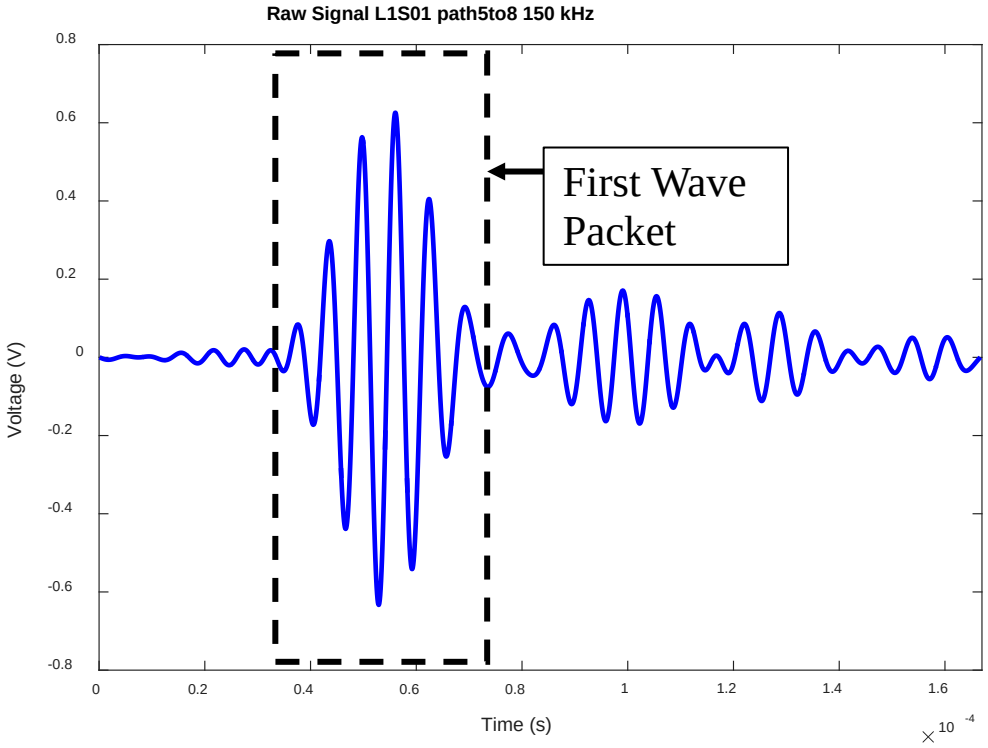

Fig. 11 Example of the raw signal and the windowed first wave packet from L1S01 path 4to9 150-kHz actuation frequency

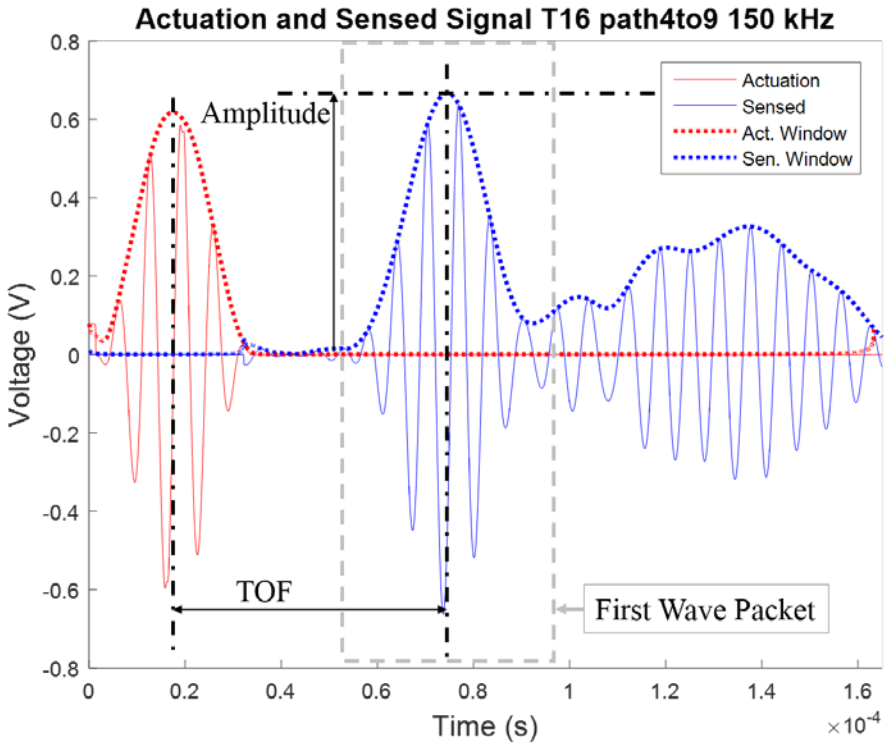

Fig. 12 Example of how the time domain features of TOF and amplitude are calculated from the sensed signal by using the envelopes of the waveforms path 4to9 150-kHz actuation frequency

The amplitude relates to the amount of displacement caused by the propagating Lamb wave and is complexly related to the structural properties and attenuation caused by the material. Signal amplitude changes were extracted using Eq. 1, where *s* is the sensed signal and *H* is the Hilbert transform, which finds the envelope of the signal

$$A = \max(|H(s)|). \tag{1}$$

TOF is the measure of the length of time taken by an actuation signal to reach a sensor. The TOF gives a sense of the Lamb wave velocity, which is related to the material properties of the composite. The TOF calculation is given in Eq. 2 where *a* is the actuation signal and *t* is elapsed time.

$$TOF = t(\max(|H(s)|)) - t(\max(|H(a)|)). \tag{2}$$

The data can also be analyzed in the frequency domain by taking the short-time Fourier transform (STFT) of the sensor signal, as show in Eq. 3 where *S*(*n*) is the signal, *F* is the sampling frequency, and *m* is the discrete size of the window *w*. For each actuation frequency ω a STFT was performed to extract frequency-domain

features. The features examined were the maximum power spectral density (PSD) value, shown in Eqs. 4 and 5, and the total energy of the wave packet, shown in Eq. 6. An example of the calculated total PSD of a signal (as in Eq. 4) and the PSD extracted at a certain frequency (as used to find the maximum in Eq. 5) are shown in Figs. 13 and 14, respectively.

$$STFT[S(n)] = S(m,\omega) = \sum_{n=-\infty}^{\infty} s(n)w(n-m)e^{-j\omega n}, \quad (3)$$

$$PSD[S(n)] = P(m,\omega) = \frac{|S(m,\omega)|^2}{F\sum_{n=1}^{L}|w(n)|^2}, \quad (4)$$

$$PSDpeak(\omega) = \max\big(P(m,\omega)\big), \quad (5)$$

and

$$Energy(\omega) = \sum_m P(m,\omega). \quad (6)$$

When used in analysis, all features are normalized by their corresponding baseline value for that path and that sample. In this way comparisons between coupons can be made and some of the variability effects between coupons are filtered out. These features were then analyzed to find one, combinations, and/or ratios that are sensitive to applied load or damage. Ideally, differing features that are more sensitive to one or the other effect can be identified so that different combinations of features can be used to diagnose applied load, classify damage type, and quantify damage severity.

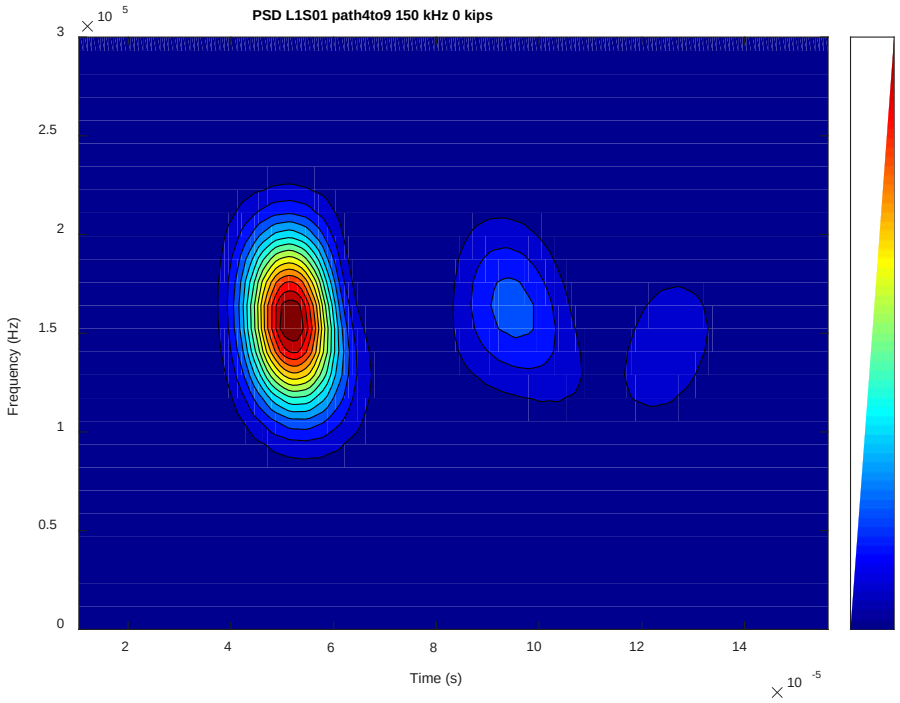

Fig. 13 Example of the PSD of L1S01 path 4to9 150-kHz actuation under a 0-kips load

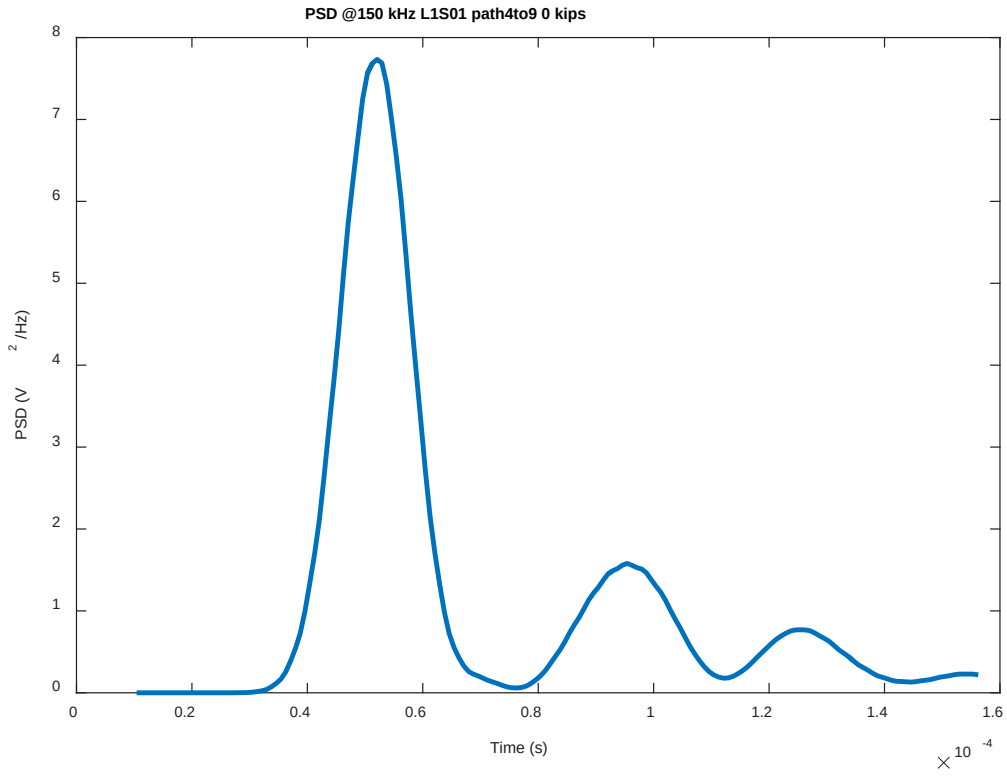

Fig. 14 Extracted PSD of the actuation frequency (150 kHz) of L1S01 path 4to9 at 0 kips (i.e., one slice at 150 kHz extracted from Fig. 13)

4. Signal Analysis

This section discusses analysis of sensed signal for effects from applied load. The goal of sensing these changes contributes toward the eventual overall goal of correctly diagnosing damage during operating conditions.

Development of accurate diagnostic algorithm requires identification of features sensitive to the effects of load-only, damage-only, and the combined effects of load-damage. Hence, the collected experimental data are analyzed for the qualitative differences driven by the effects outlined previously. Progression of applied load in the data will allow finding specific signal features that correlate to these effects.

The wave data collected in the static loading at the beginning of each test (before damage propagation has begun) contain only effects from the applied load on the coupons at increasing load levels. In analyzing these data, the actuation frequencies that resulted in clear first wave packets were narrowed down to the 3 frequencies, 150, 200, and 250 kHz, and among these 3 frequencies the data from 150 kHz actuation are the clearest. Additionally only the propagation paths, which match the loading direction ("straight" paths, which are paths 2to11, 3to10, 4to9, and 5to8 in Fig. 15) are used in the analysis to avoid complications that arise when the directions are not concurrent. As the applied load and local material properties "seen" by paths at an off-angle direction from the loading direction and orientation of the composite layup, merging all data from different orientations together with directionality compensation would be incorrect.

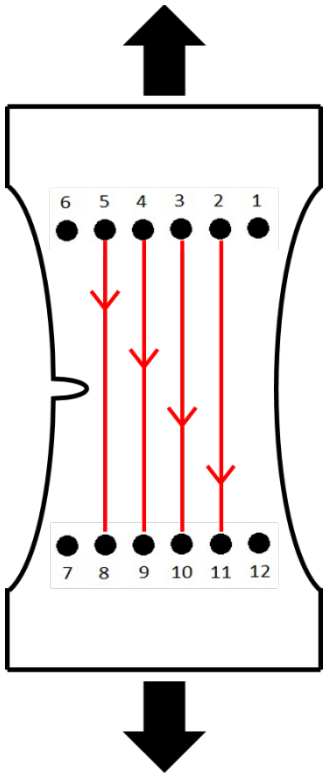

Fig. 15 Schematic showing actuator and sensor numbering and the 4 straight paths used in analysis whose direction coincides with the shown loading direction

Qualitative observations were done on the raw sensed signal to assess general signal changes and establish preliminary trends. Figure 10 shows the first wave packet of a coupon as the applied load on the coupon increases incrementally from 0 to 4 kips. It can be observed that there is a slight, steady increase in signal amplitude as the applied load increases and also a slight, steady decrease in the time the signal reaches that maximum amplitude, and therefore in the time of flight as the applied load increases. Similarly, when examining how the PSD profile changes at the actuation frequency of the signal with load in Fig. 16 an increase in the maximum PSD value and an increase in energy (the area under the curve) is observed as applied load increases.

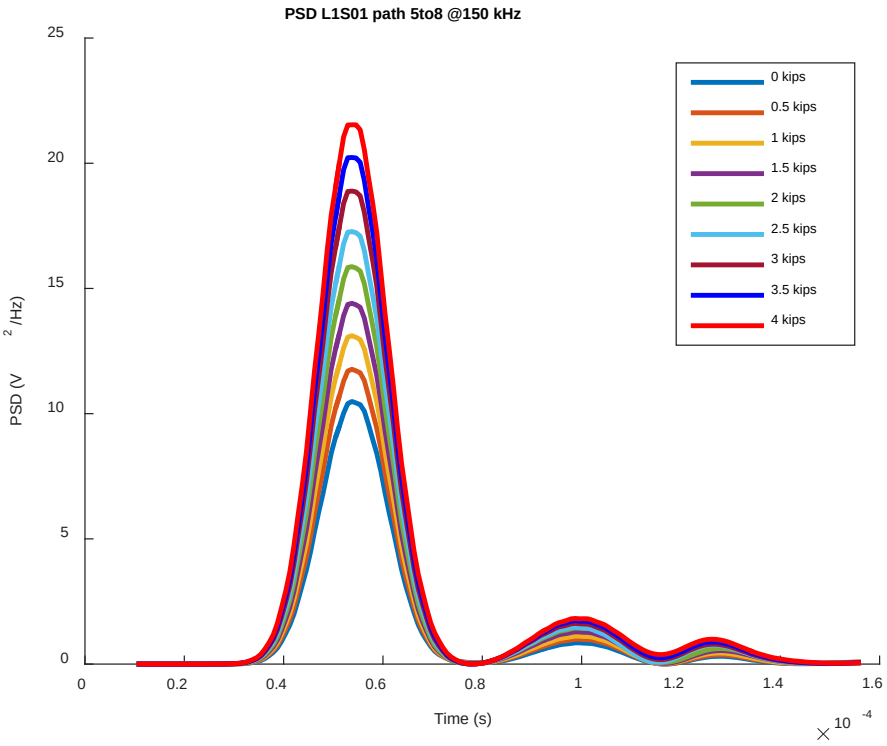

Fig. 16 Extraction of the PSD of L1S01 at the actuation frequency 150-kHz path 5to8 as applied load increases

Signal features that have been found to be most influenced by applied load are those described in the previous section: amplitude, maximum PSD value, and signal energy. Time of flight is also influenced by applied load, but less consistently than these other signal features. Plots showing the change in these 4 features (normalized to the baseline value for each coupon) as increased load is applied are shown for each straight path: amplitude of path 2to11 in Fig. 17, TOF of path 5to8 in Fig. 18, maximum PSD of path 3to10 in Fig. 19, and energy of path 4to9 in Fig. 20.

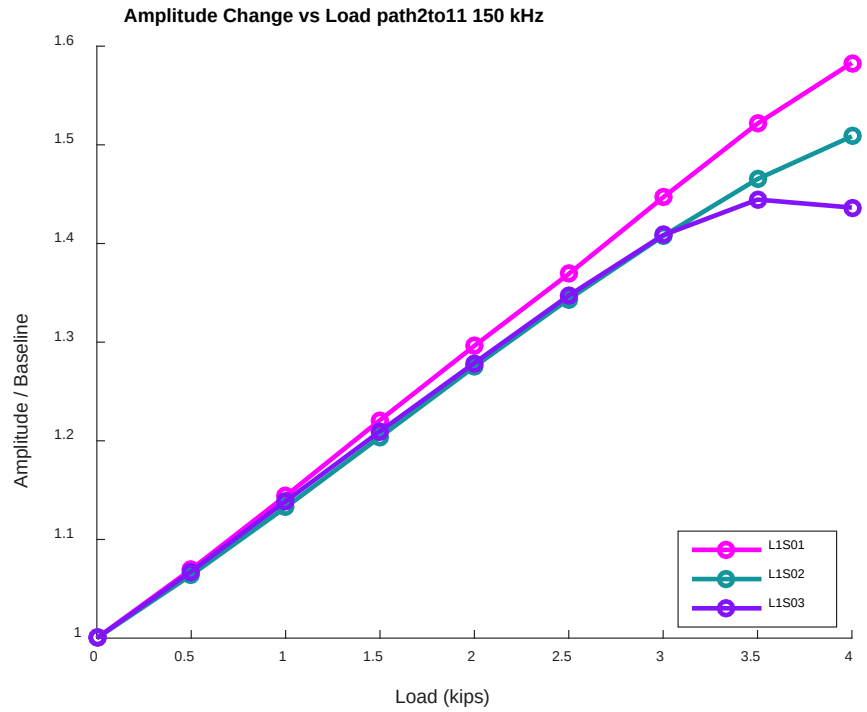

Fig. 17 Normalized amplitude change in the first wave packet of data with actuation frequency 150 kHz from path 2to11 for ARL-tested coupons

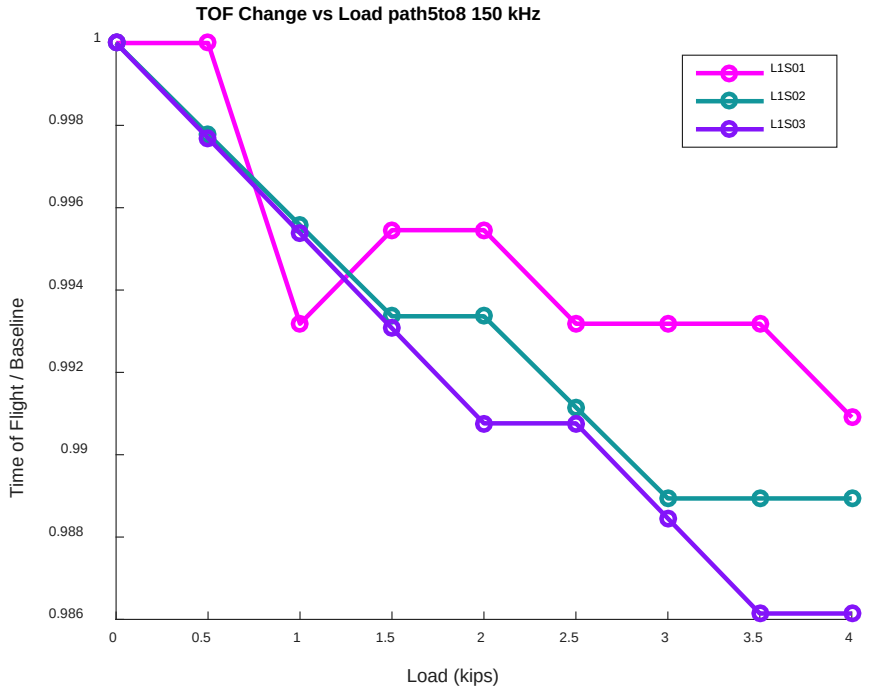

Fig. 18 Normalized TOF change in the first wave packet of data with actuation frequency 150 kHz from path 5to8

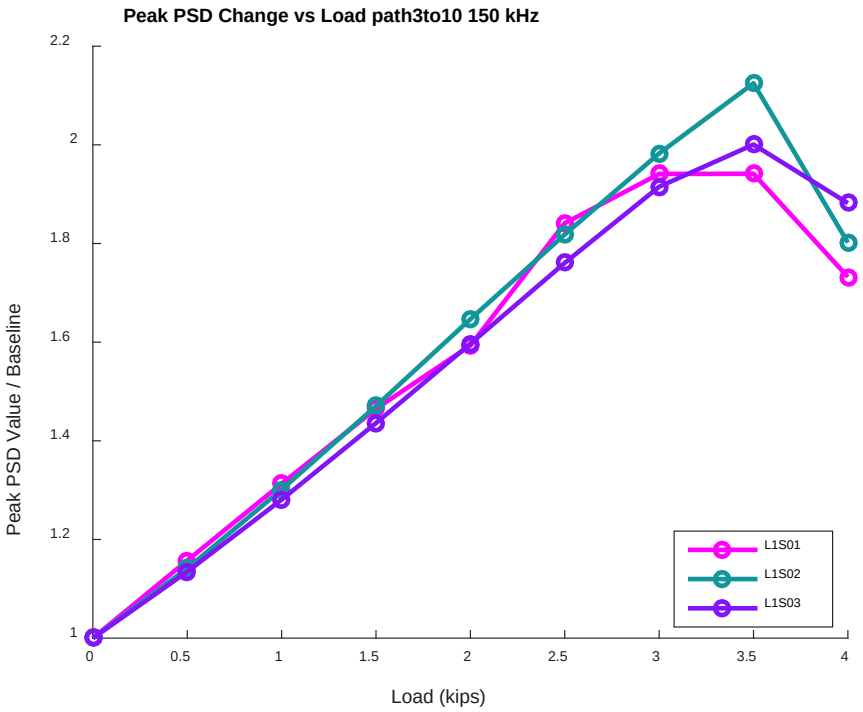

Fig. 19 Normalized maximum PSD value change in the first wave packet of data with actuation frequency 150 kHz from path 3to10

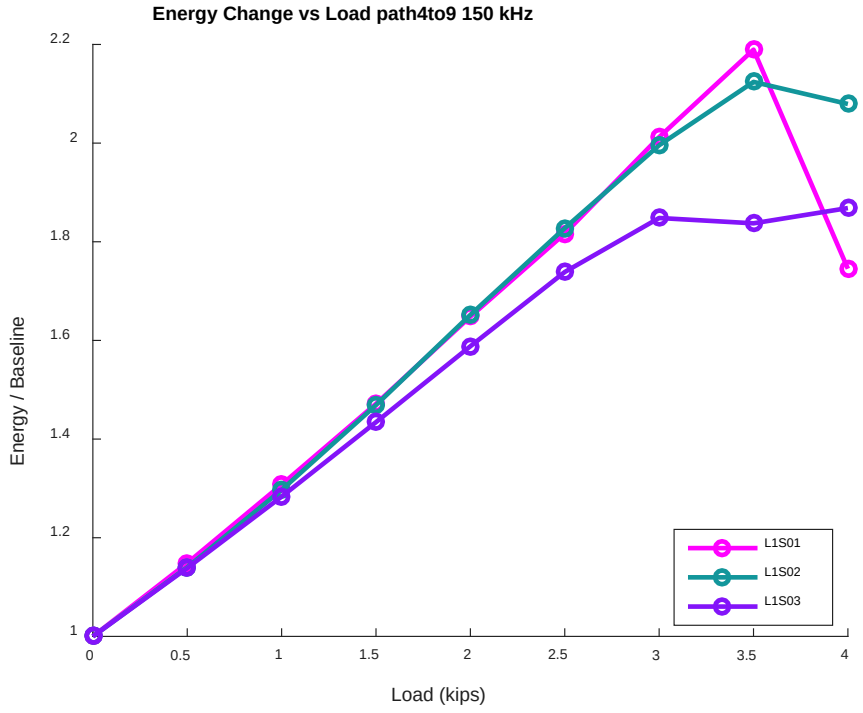

Fig. 20 Normalized energy change in the first wave packet of data with actuation frequency 150 kHz from path 4to9

Figures 17, 19, and 20 show that above 3 kips load inflection points begin to appear in the data—this is indicative of damage initiation and progression. Based on Figs. 17–20 and similar plots from other paths and actuation frequencies, X-ray images taken after the initial loading cycle, and notes about audible cracking during tests, it can be hypothesized that matrix cracking can begin in a sample between 2.5- and 4-kips load. By filtering out data beyond these inflection points (based on the hypothesis that they are also affected by damage), Lamb wave data influenced only by applied load can be isolated. This will be done when creating modeling strategies to predict applied load from ultrasonic data, as only data with applied load influences and not those from the combined influences of applied load and data should be used for this inverse problem.

5. Conclusions and Future Work

From the results in previous sections, a clear effect is observed from applied load on the ultrasonic wave data. Using these trends, mathematical models that estimate the applied load from the sensor signal can be developed. By combining the data shown in this report with previous work by the authors, multiple linear regression models using various combinations of the sensor signal features as predictors for the applied load can be trained and tested. These models will be a part of a future work.

6. References

1. Michaels K. Market trends: aerospace composites market will quadruple by 2026. Composites World; n.d. [accessed 2007 July]. http://www.compositesworld.com/columns/market-trends-aerospace-composites-market-will-quadruple-by-2026.

2. Soutis C. Recent advances in building with composites. Plast Rubber Compos. 2009;38(9–10):359–366.

3. Williams A. Aerospace growth climbs with carbon fiber. Composites World; n.d. [accessed 2016 July 12]. http://www.compositesworld.com/columns/aerospace-growth-climbs-with-carbon-fiber.

4. Curtis PT, Dorey G. Fatigue of composite materials. In: Proc Instn Mech Engrs, Part G. J Aero Engr. 1989;203(1):31–37.

5. Gay D. Composite materials: design and applications. 3rd ed. Boca Raton (FL): CRC Press; 2014.

6. Soutis C. Carbon fiber reinforced plastics in aircraft construction. Mater Sci Eng A. 2005;412(1–2):171–176.

7. Yancey R. Laminated composites: The original additive manufacturing process. Composites World; n.d. [accessed 2016 Mar]. http://www.compositesworld.com/articles/laminated-composites-the-original-additive-manufacturing-process.

8. Kollar LP, Springer GS. Mechanics of composite structures. New York (NY): Cambridge University Press; 2003.

9. Beaumont PWR, Dimant RA, Shercliff HR. Failure processes in composite materials: getting physical. J Mater Sci. 2006;41(20):6526–6546.

10. Poursartip A, Ashby MF, Beaumont PWR. The fatigue damage mechanics of a carbon fibre composite laminate: I-development of the model. Compos Sci Technol. 1986;25(3):193–218.

11. Waddoups ME, Eisenmann JR, Kaminski BE. Macroscopic fracture mechanics of advanced composite materials. J Compos Mater. 1971;5(4):446–454.

12. Wisnom MR, Chang F-K. Modelling of splitting and delamination in notched cross-ply laminates. Compos Sci Technol. 2000;60(15):2849–2856.

13. Talreja R. Damage mechanics and fatigue life assessment of composite materials. Int J Damage Mech. 1999;8:339–354.

14. Hallett SR, Jiang WG, Khan B, Wisnom MR. Modelling the interaction between matrix cracks and delamination damage in scaled quasi-isotropic specimens. Compos Sci Technol. 2008;68(1):80–89.

15. Starke EAJ, Cornelia RH, Greszczuk LG, Karabin LM, Lewandowski JJ, Saxena A, Seferis JC, Tressler RE, Ward DD. Accelerated aging of materials and structures. The effects of long-term elevated-temperature exposure. Washington (DC): National Academy Press; 1996.

16. O'Brien TK. Characterization of delamination onset and growth in a composite laminate. Hampton (VA): Langley Research Center; 1982. NASA Tech Report.: NASA-TM-81940.

17. Scott IG, Scala CM. A review of non-destructive testing of composite materials. NDT Int. 1982;15(2):75–86.

18. Sloan J. The NDE challenge. Composites World; n.d. [accessed 2016 May]. http://www.compositesworld.com/columns/the-nde-challenge.

19. Cawley P. Inspection of composites – current status and challenges. In: 9th European Conference on Nondestructive Testing; 2006 Sep 25–29; Berlin, Germany.

20. Gholizadeh S. A review of non-destructive testing methods of composite materials. In: Procedia structural integrity. 2016;1:50–57.

21. Liu B, Lessard LB. Fatique and damage-tolerance analysis of composite laminates: Stiffness loss, damage-modelling, and life prediction. Compos Sci Technol. 1994;51:43–51.

22. Farrar CR, Worden K. An introduction to structural health monitoring. Philos Trans R Soc A. Math Phys Eng Sci. 2007;365(1851):303–315.

23. Haile MA, Hall AJ, Yoo JH, Coatney MD, Myers OJ. Detection of damage precursors with embedded magnetostrictive particles. J Intel Mater Syst Struct. 2015;27(12):1567–1576.

24. Haile MA, Riddick JC, Assefa AH. Robust particle filters for fatigue crack growth estimation in rotorcraft structures. IEEE Trans Reliability. 2016;65:1438–1448.

25. Haile M, Ghoshal A. Application of compressed sensing in full-field structural health monitoring. In: Proc. SPIE 8346, Smart Sensor Phenomena, Technology, Networks, and Systems Integration; San Diego (CA). 2012. p. 46–53.

26. Haile MA, Ifju PG. Application of elastic image registration and refraction correction for non-contact underwater strain measurement. Strain. 2012;48(2):136–142

27. Haile MA, Chen TK, Sediles F, Le D. Estimating crack growth in rotorcraft structures subjected to mission load spectrum. Int J Fatigue. 2012;43:142–149.

28. Leo DJ. Piezoelectric materials. In: Engineering analysis of smart material systems. 1st ed. Hoboken, (NJ): John Wiley & Sons; 2007. p. 122–204.

29. Worden K. Rayleigh and lamb waves - basic principles. Strain. 2001;37(4):167–172.

30. Su Z, Ye L, Lu Y. Guided lamb waves for identification of damage in composite structures: a review. J Sound Vib. 2006;295(3–5):753–780.

31. Williams WB, Michaels TE, Michaels JE. Characterization of guided wave velocity and attenuation in anisotropic materials from wavefield measurements. In: 42nd Annual Review of Progress in Quantitative Nondestructive Evaluation (QNDE), AIP Conf. Proc; 1706, 2016. vol. 1706. p. 30002.

32. Harris B. Fatigue in composites: science and technology of the fatigue response of fibre-reinforced plastics. 1st ed. Boca Raton (FL): Woodhead Publishing Ltd; 2003.

33. Larrosa CC. Monitoring matrix cracking in composite laminates using built-in piezoelectric sensors. Stanford (CA): Stanford University; 2013.

34. Lin M, Qing XP, Kumar A, Beard SJ. SMART layer and SMART suitcase for structural health monitoring applications. In: Proc. SPIE 4332, smart structures and materials 2001: industrial and commercial applications of smart structures; 2001. vol. 4332. p. 98–106.

List of Symbols, Abbreviations, and Acronyms

3-D	3-dimensional
AE	acoustic emission
ARL	US Army Research Laboratory
CT	computed tomography
MTS	mechanical testing system
NDE	nondestructive evaluation
PSD	power spectral density
PZT	lead zirconate titanate
SHM	structural health monitoring
STFT	short-time Fourier transform
TOF	time of flight

1 (PDF) DEFENSE TECHNICAL INFORMATION CTR DTIC OCA

2 (PDF) DIRECTOR US ARMY RESEARCH LAB RDRL CIO L IMAL HRA MAIL & RECORDS MGMT

1 (PDF) GOVT PRINTG OFC A MALHOTRA

4 (PDF) DIR USARL RDRL VT E RIGAS RDRL VTM C ROSANIA M HAILE J RIDDICK